Journal of Modern Optics
Publication details, including instructions for authors and subscription information:
http://www.tandfonline.com/loi/tmop20

High field broadband THz generation in organic materials

C. Vicario [a] , C. Ruchert [b] & C.P. Hauri [a b]
[a] Paul Scherrer Institute , 5232 Villigen PSI , Switzerland
[b] Ecole Polytechnique Federale de Lausanne , 1015 Lausanne , Switzerland
Published online: 31 May 2013.

To cite this article: C. Vicario , C. Ruchert & C.P. Hauri (2013): High field broadband THz generation in organic materials, Journal of Modern Optics, DOI: 10.1080/09500340.2013.800242

To link to this article: http://dx.doi.org/10.1080/09500340.2013.800242

Journal of Modern Optics, 2013
http://dx.doi.org/10.1080/09500340.2013.800242

Taylor & Francis
Taylor & Francis Group

High field broadband THz generation in organic materials

C. Vicario[a]*, C. Ruchert[b] and C.P. Hauri[a,b]

[a]*Paul Scherrer Institute, 5232 Villigen PSI, Switzerland;* [b]*Ecole Polytechnique Federale de Lausanne, 1015 Lausanne, Switzerland*

(*Received 31 January 2013; final version received 23 April 2013*)

Organic salt crystals, e.g. DAST, OH1, and DSTMS, pumped by ultra-short infrared laser are efficient THz emitters. We review our latest results on the generation in organic crystals of THz single-cycle transients with field strength of 1.5 MV/cm. The energy conversion reaches 2% with photon conversion efficiency up to 200%. THz radiation produced in such crystals offers excellent beam propagation properties and can be focused down to diffraction limited spot size in order to realize the highest field. This source covers the full spectral range between 0.1 and 10 THz. Further, we discuss the possibility to control the absolute phase and the polarity of the THz field.

Keywords: THz generation; organic crystal; terahertz gap

1. Introduction

Terahertz (THz) radiation located between the optical and the microwave frequency region known as the THz gap (0.1–10 THz) is well suited to explore fundamental physical phenomena and to drive applications in biology, homeland security, and medicine [1]. High strength THz fields hold the promise of new insights in magnetization dynamics, collective effects in gas and solids, charged particle manipulations, and high harmonic generation [2]. High-peak THz transients are also a versatile tool at X-ray free electron laser facilities, for novel pump and probe experiments as well as for the temporal characterization of the X-ray pulse on the femtosecond time scale [3,4].

While high field transients at frequencies between 20 and 100 THz (15 μm–3 μm) have been demonstrated in inorganic crystals [5], the generation of few-cycle or even single-cycle fields exceeding 1 MV/cm in the THz gap has remained challenging [6,7]. Recently, with a THz source based on $LiNbO_3$, a field of 1 MV/cm [6] has been demonstrated with the potential to reach sub-mJ pulse energy with cryogenic cooled crystals [8]. In this material, the emitted spectrum appears to be confined to frequency range typically around or below 1 THz. To access significantly higher frequencies, we recently developed a compact and powerful laser-driven THz source based on organic emitters. The radiation is generated by optical rectification in organic salt crystals such as DAST [9], OH1 [10], and DSTMS [11]. The THz is realized with a phase matched nonlinear $\chi^{(2)}$ process [12]. Different spectral components of the laser, with relative offset $\Delta\omega$, drive nonlinear polarization and emission pulses at frequency $\omega_{THz} = \Delta\omega$. For optical rectification, the generated pulses are characterized by stable absolute phase. Values of ω_{THz} covering the full THz gap become possible for a broadband laser spectrum and a crystal supporting this bandwidth. The optical rectification in organic salt materials permits the realization of extremely intense and broadband THz electromagnetic fields [9–11]. These materials provide in fact low THz absorption and $\chi^{(2)}$ one order of magnitude larger than room temperature $LiNbO_3$. Velocity matching is achieved in a collinear geometry for pump wavelengths between 1.35 and 1.5 μm. The crystals can be anti-reflection coated, and their damage threshold for femtosecond pulses exceeds 160 GW/cm^2. THz radiation is emitted collinearly to the pump with excellent focusing characteristics. The phase velocity mismatch and the THz re-absorption determine the optimal thickness of the organic crystal. Thus, for a suitably thin crystal, as reported in the following, the output spectrum extends to the full THz gap.

2. Experimental setup

The experimental setup is shown in Figure 1(*a*), while a detailed description is provided elsewhere [9]. In brief, a TW-class Ti:Sa laser at 100 Hz, producing 60 fs FWHM pulses, drives an optical parametric amplifier (OPA) and provides at the same time a sub-μJ probe at 800 nm for electro-optical sampling (EOS). The OPA generates pulses with 70 fs FWHM duration and up to 2.5 mJ at

*Corresponding author. Email: carlo.vicario@psi.ch

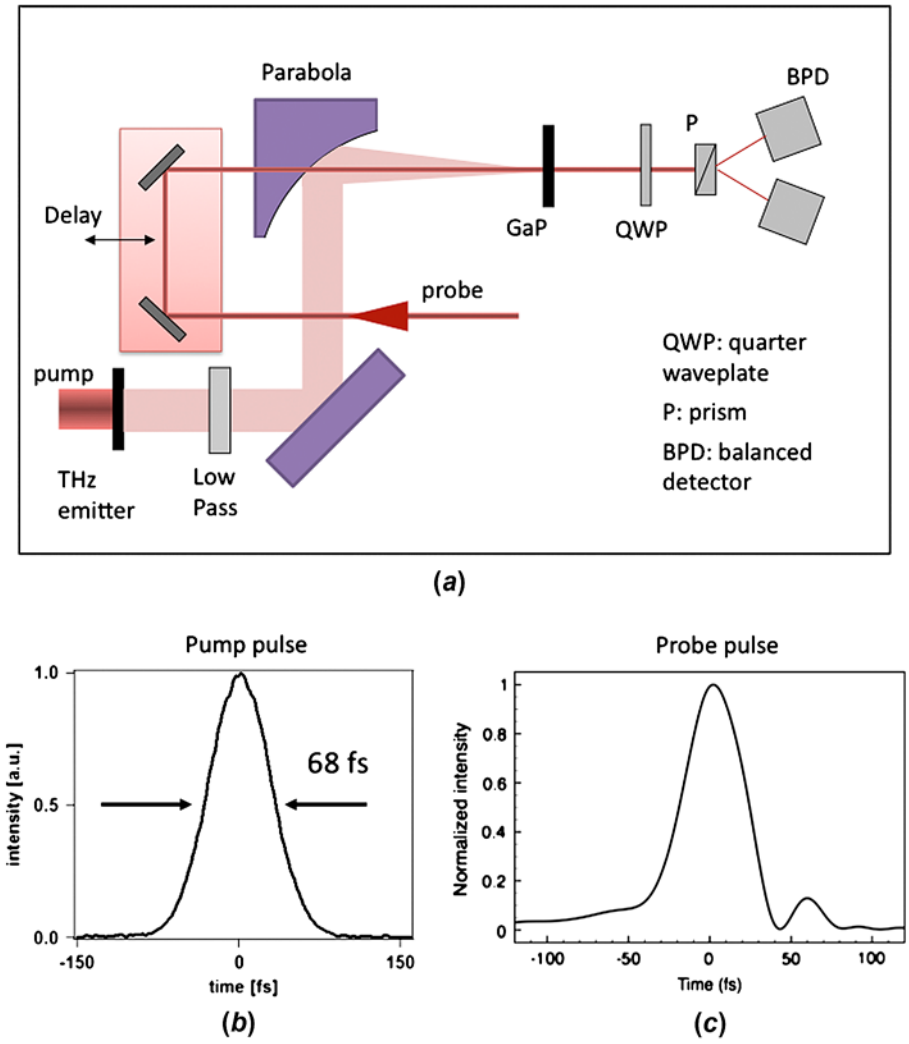

Figure 1. (*a*) Experimental setup for the THz generation and detection (from [9]). (*b*) A short pump pulse from an optical parametric amplifier drives optical rectification in the organic crystal. Standard electro-optical sampling with (*c*) a short 800 nm probe is used for temporal and spectral characterization. (The color version of this figure is included in the online version of the journal.)

the IR wavelengths required for THz generation in organic crystals. The THz is emitted from thin organic crystals collinearly to the pump. Behind the organic crystal, a thin sheet of Teflon or blackened Topas polymer selectively blocks the residual IR beam. The beam is expanded and then tightly focused by an off-axis parabolic (OAP) mirror (f = 101.6 mm) for electro-optical sampling. The EOS gives direct access to the THz electric field shape, the peak electric field, and the spectral content. The electro-optical spectral sensitivity for our electro-optical setup (GaP with 95 µm thickness) decreases above 5 THz with frequency cut-off at 7 THz. The cut-off in the detection crystal is determined mainly by the group velocity mismatching between THz and optical probe [13] and by the electro-optical spectral response [14]. THz pulses with spectral components beyond 5 THz are measured by means of Fourier transform first order interferometry. It is realized in a Michelson interferometer equipped with Golay cell detectors [15]. The pellicle beam splitter installed in the interferometer is suitable for radiation in the frequency range 0.7–20 THz. Absolute energy measurements are carried out by means of a calibrated Golay cell equipped with diamond entrance window (produced by Tydex) and of a pyroelectric deuterated triglycine sulfate detector (DTGS model D201 manufactured by Bruker). The Golay cell sensitivity has been calibrated in energy up to 12 THz using a blackbody source. The transverse beam profile is recorded with a bolometer un-cooled camera having a pixel size of 23.5 µm.

In this paper, we report intense single-cycle THz transients generated in the organic crystals DAST, DSTMS, and OH1. In order to prevent crystal damage while using the maximum available pump flux, large crystals with up

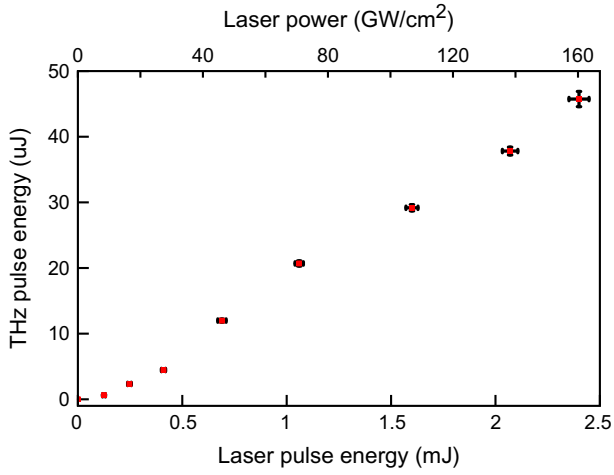

Figure 2. THz energy generated from 8 mm aperture DAST crystal as function of infrared pump energy and power density. Energy stability of the THz pulse is comparable to the pump energy stability and equal to 1% rms. (The color version of this figure is included in the online version of the journal.)

to 10 mm aperture at a nominal thickness of 0.5 mm have been utilized. On the other hand, thinner crystals are shown to be adequate for the generation of multi-octave spanning spectra covering the entire THz gap.

3. Experimental results

3.1. Energy conversion efficiency studies

In Figure 2, the THz pulse energy generated in a 0.5 mm thick DAST crystal with an aperture of 8 mm is shown as a function of the infrared laser energy and power density. The temporal shape of the THz pulse is determined through EOS in a GaP crystal. The absolute THz energy is determined by the Golay cell positioned after the low-pass filter and energy-calibrated THz attenuators. Maximum THz pulse energy $E_{THz} = 45\ \mu J$ is reached when the crystal is pumped by $E_{IR} = 2.4$ mJ (at 160 GW/cm^2). The experimental points confirm that the crystal is operated far from the saturation. The pump-to-THz energy conversion ($\eta_E = E_{THz}/E_{IR}$) is about 2%. This corresponds to a photon conversion efficiency η_{ph} larger than 200% ($\eta_{ph} = 100N_{THz}/N_{IR}$, where N_{THz} and N_{IR} are the number of photons for the THz and the IR pump pulses) [9]. Furthermore, the shot-to-shot THz energy stability is

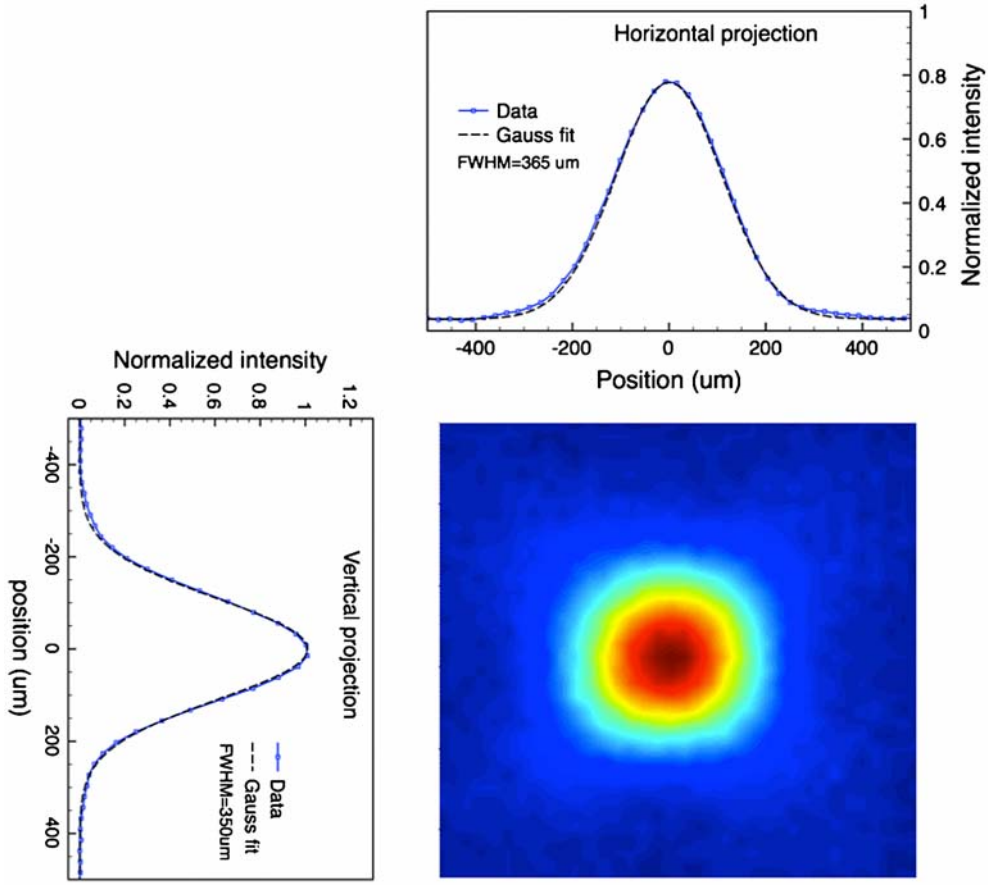

Figure 3. Focused THz generated in DSTMS together with vertical and horizontal projections and Gaussian fit. The beam, recorded with a micro-bolometer camera, indicates vertical and horizontal FWHM of 350 and 366 μm. (The color version of this figure is included in the online version of the journal.)

remarkable. The energy variation recorded over 500 consecutive shots is better than 1% rms comparable to the OPA energy stability (see error bars of Figure 2). The quasi-linear dependence of the generated energy indicates that the upscale of the THz output by increasing the source energy is further feasible. It is worth noting that the maximum power density of 160 GW/cm^2 used is not inducing damages in the organic crystal. For other organic materials, the THz energy yield recorded in the same experimental conditions is approximately 1%.

3.2. *THz focus characteristics*

The THz generation occurs over several millimeters of crystal area illuminated by the pump. The THz beam therefore has a divergence of only a few mrad. In our setup, tight focusing is ensured by a 10 cm focal length parabola placed about 2 m from the THz organic crystal. In Figure 3, we show the THz transverse intensity profile produced in an 8 mm aperture DSTMS crystal. The profile was recorded with an un-cooled bolometer array sensor. The focus shape is circular and not affected by

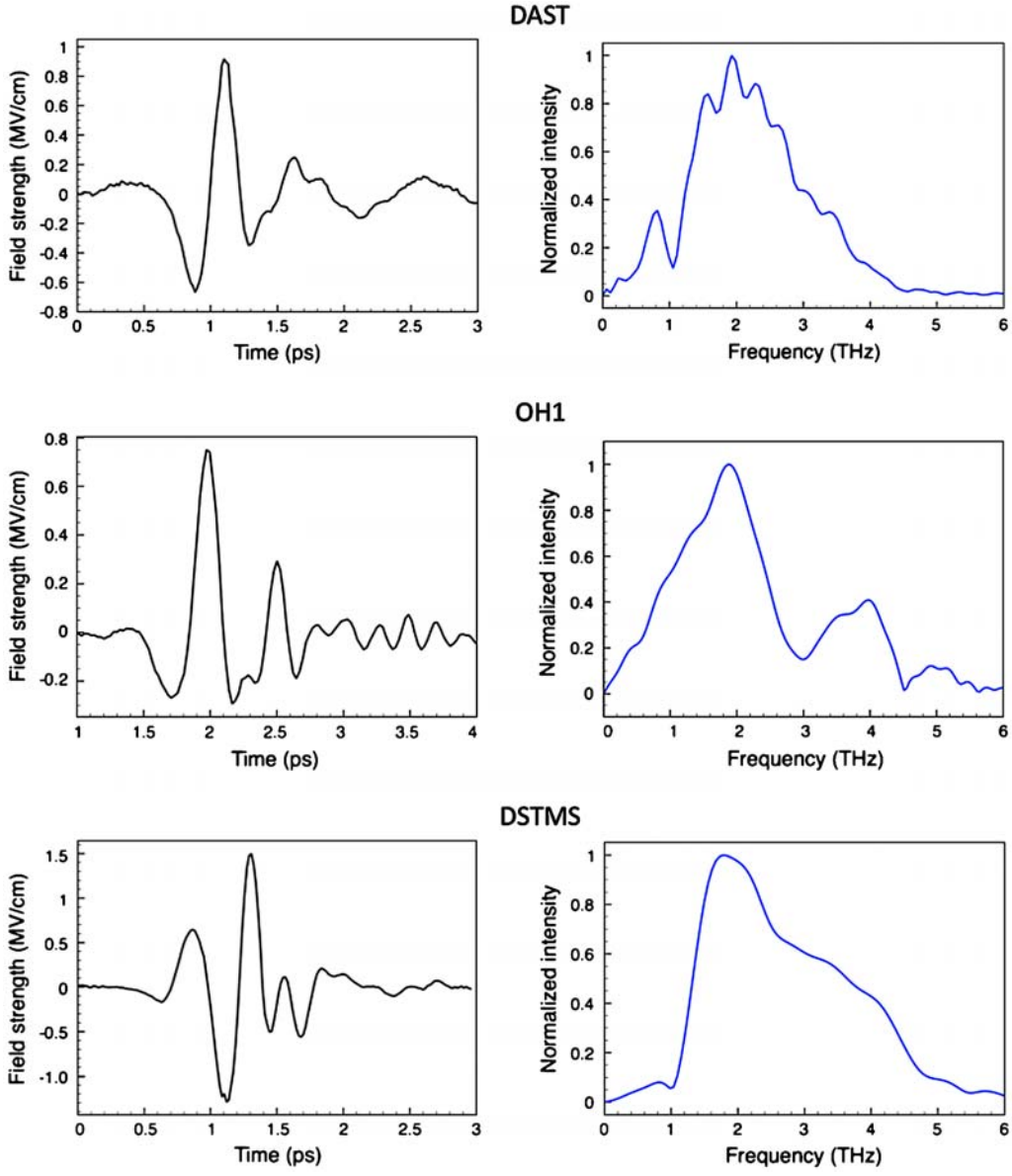

Figure 4. Temporal (left) and spectral shapes (right) of the THz radiation emitted by different organic crystals. The radiation is generated in approximately same thickness crystals: 0.43, 0.4, and 0.49 mm for DAST, OH1, and DSTMS, respectively. In all the case the optical rectification process is driven by IR pump at power densities up to160 GW/cm^2. (The color version of this figure is included in the online version of the journal.)

astigmatism or other visible aberrations. As shown in the projected profiles, the intensity is well fitted by a Gaussian with full width half maximum (FWHM) of 360 μm, which is close to the diffraction limit. The beam size measurement carried out for other organic crystals also resulted in excellent focusing characteristics. The foci are somewhat larger but still in the order of sub-mm.

3.3. THz field with MV/cm strength

The temporal shapes of the THz radiation for DAST, DSTMS, and OH1 are shown in Figure 4 (left plots). High energy per pulse concentrated in one or two optical cycles and very tight focusing, reported before, allow for high THz field. The peak electric field is calibrated against the THz electro-optical effect and crosschecked with fluence and pulse duration measurement [9]. The spectral intensity, right side plots in Figure 4, is calculated by Fourier transformation of the corresponding temporal evolution. For all the crystals, the THz transient approximates a single-cycle temporal oscillation with different grade of asymmetry. The maximum field recorded for DSTMS displays a peak of 1.5 MV/cm and magnetic field of 0.5 T. For OH1 and DAST organic crystals, the peak field is slightly less than 1 MV/cm when pumped by the same pump fluence. With respect to OH1 and DAST, the higher frequencies for DSTMS result in a tighter focus and shorter THz pulse and thus in higher peak field. The calculated spectra reveal the absorption properties and phonon resonances of each organic material, as reported in literature [16–18]. Due to these absorptions, the temporal transients exhibit oscillations after the main pulse.

3.4. Control of the THz absolute phase

The THz pulse generated by optical rectification is characterized by a stable absolute phase. This is an important feature for field-sensitive applications. Equally important, for exploring nonlinear dynamics, is the generation of the highest field at the interaction by proper control of the absolute phase of the single/few cycle THz pulses. In fact, for the highest asymmetry and zero absolute offset, the THz pulse could potentially act as a quasi-unipolar stimulus. We demonstrated recently an efficient method to directly control the absolute phase of a THz pulse by combining dispersion properties of different transparent plastics [11]. Teflon and Topas polymer sheets with different thickness were used in order to vary the THz absolute phase and forming a fully asymmetric pulse, as shown in Figure 5. The energy losses and the peak field reduction associated with such phase manipulation are negligible. To the best of our knowledge, the absolute phase control for THz pulses has not been demonstrated so far for such multi-octave spanning spectra. Moreover, in our setup, the THz field polarity can be easily inverted by 180° rotation of the organic crystal.

3.5. Ultra-broadband THz generation

Both the phase velocity mismatch and the THz re-absorption define the optimal thickness of the organic crystal and therefore the THz spectral content. For the generation of high frequencies, thin crystals are necessary. In Figure 6, the broadband spectrum generated via optical rectification in 180 μm thick DAST is presented. To avoid the decrease of sensitivity caused by the

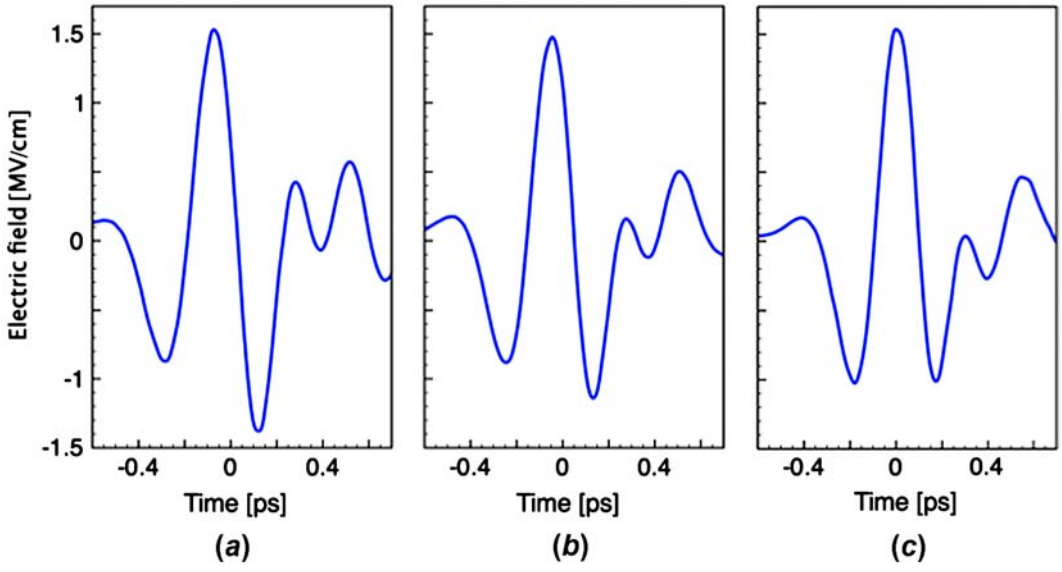

Figure 5. Direct manipulation of the absolute phase of the THz pulse by dispersion management by means of transparent plastic. The pulses are characterized by a carrier envelope phase offset of (*a*) π/3 rad, (*b*) π/6 rad, and (*c*) zero. (The color version of this figure is included in the online version of the journal.)

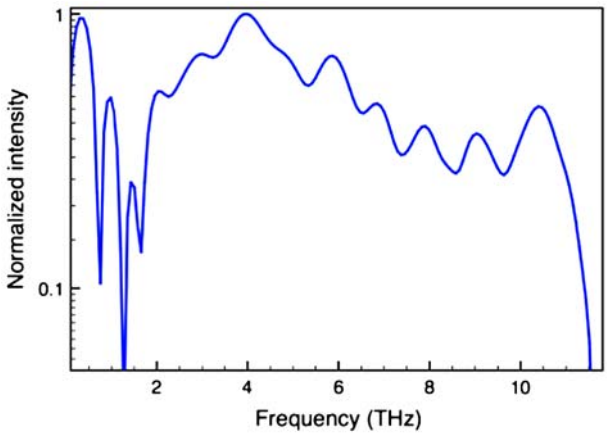

Figure 6. Spectrum generated in 180 μm DAST crystal and reconstructed with first order autocorrelation. The generated spectrum is relatively flat and extends over the full THz gap. Several absorption peaks due to phonon resonances in the organic crystal are visible. (The color version of this figure is included in the online version of the journal.)

electro-optic detection (at frequencies higher than 5 THz), the spectra are reconstructed by Fourier interferometry. Moreover, for these measurements, the low pass Teflon filter, which is transparent to up to 5 THz, is replaced by blackened home-developed Topas polymer, which is characterized by low absorption in the entire THz gap [19]. The measured spectra are impressively large and extend far beyond 10 THz. With organic crystals it is possible to produce high fields in the whole THz gap (0.1–10 THz) and, furthermore, it seems feasible to extend the spectral region up to frequencies only accessible by optical difference frequency generation (>20 THz).

4. Conclusions

In this paper, we have reviewed OH1, DAST, and DSTMS organic crystals in view of their potential of high-field generation in the THz gap (0.1–10 THz). All crystals turned out to be highly efficient (up to 2% energy conversion yield) and broadband THz emitters when pumped by a mJ femtosecond infrared pulse. The generated THz radiation offers multi-octave spanning, single-cycle, and phase-stable pulses with up to 1.5 MV/cm electric and 0.5 T magnetic field strength. The generation scheme based on a collimated pumping geometry provides excellent THz focusing characteristics. We have discussed a new method to efficiently control the absolute phase and the polarity of the THz field. Ultra-broadband THz spectra covering the frequency range 1–10 THz could be realized by optical rectification in a thin organic crystal. The THz source presented here will be of benefit for field-sensitive investigations to drive extreme nonlinear phenomena in gases and solids with single-cycle transients.

Acknowledgements

We acknowledge support from the Swiss National Science Foundation (grant nos. PP00P2128493 and 20002-1122111) and SwissFEL. CPH acknowledges association to NCCR-MUST. We thank C. Erny for useful discussion.

References

[1] Tonouchi, M. *Nat. Photonics* **2007,** *1,* 97–105.
[2] Balogh, E.; Kovacs, K.; Dombi, P.; Fulop, J.A.; Farkas, G.; Hebling, J.; Tosa, V.; Varju, K. *Phys. Rev. A: At., Mol., Opt. Phys.* **2011,** *84,* 023806.
[3] Hoffmann, M.C.; Turner, J.J. *Synchrotron Radiat. News* **2012,** *25*(2)*,* 17–24.
[4] Fruehling, U.; Wieland, M.; Gensch, M.; Gebert, T.; Schuette, B.; Krikunova, M.; Kalms, R.; Budzyn, F.; Grimm, O.; Rossbach, J.; Ploenjes, E.; Drescher, M. *Nat. Photonics* **2009,** *3,* 523–528.
[5] Jungiger, F.; Sell, A.; Schubert, O.; Mayer, B.; Brida, D.; Marangoni, M.; Cerullo, G.; Leitenstorfer, A.; Huber, R. *Opt. Lett.* **2010,** *35,* 2645–2647.
[6] Hirori, H.; Doi, A.; Blanchard, F.; Tanaka, K. *Appl. Phys. Lett.* **2011,** *98,* 091106.
[7] Daranciang, D.; Goodfellow, J.; Fuchs, M.; Wen, H.; Ghimire, S.; Reis, D.A.; Loos, H.; Fisher, A.S.; Lindenberg, A.M. *App. Phys. Lett.* **2011,** *99,* 141117.
[8] Fülöp, J.A.; Pálfalvi, L.; Klingebiel, S.; Almási, G.; Krausz, F.; Karsch, S.; Hebling, J. *Opt. Lett.* **2012,** *37,* 557–559.
[9] Hauri, C.P.; Ruchert, C.; Ardana, F.; Vicario, C. *Appl. Phys. Lett.* **2011,** *99,* 161116.
[10] Ruchert, C.; Vicario, C.; Hauri, C.P. *Opt. Lett.* **2012,** *37,* 899–901.
[11] Ruchert, C.; Vicario, C.; Hauri, C.P. *Phys. Rev. Lett.* **2013,** *110,* 123902.
[12] Bass, M.; Franken, P.A.; Ward, J.F. *Phys. Rev. A* **1965**, *138*, 534–542.
[13] Wu, Q.; Zhang, X.C. *Appl. Phys. Lett.* **1997,** *70,* 1784–1786.
[14] Faust, W.L.; Henry, C.H. *Phys. Rev. Lett.* **1966,** *17,* 1265–1268.
[15] RadiaBeam Technologies Home Page. http://www.radiabeam.com (accessed Jan 10, 2013).
[16] Schneider, A.; Neis, M.; Stillhart, M.; Ruiz, B.; Khan, R. U.A.; Günter, P. *J. Opt. Soc. Am. B* **2006,** *23,* 1822–1835.
[17] Brunner, F.D.J.; Kwon, O.-P.; Kwon, S.; Jazbinsek, M.; Schneider, A.; Günter, P. *Opt. Express* **2008,** *16,* 16496–16508.
[18] Mutter, L.; Brunner, F.D.; Yang, Z.; Jazbinsek, M.; Günter, P. *J. Opt. Soc. Am. B* **2007,** *24,* 2556–2561.
[19] Cunningham, P.D.; Valdes, N.N.; Vallejo, F.A.; Hayden, L.M.; Polishak, B.; Zhou, X.-H.; Luo, J.; Jen, A.K.-Y.; Williams, J.C.; Twieg, R.J. *J. Appl. Phys.* **2011,** *109,* 043505.